Biochemical characterization of the Pseudomonas putida 3-hydroxyacyl ACP:CoA transacylase, which diverts intermediates of fatty acid de novo biosynthesis

THE JOURNAL OF BIOLOGICAL CHEMISTRY
Vol. 277, No. 45, Issue of November 8, pp. 42926–42936, 2002

Printed in U.S.A.

Biochemical Characterization of the *Pseudomonas putida* 3-Hydroxyacyl ACP:CoA Transacylase, Which Diverts Intermediates of Fatty Acid *de Novo* Biosynthesis*

Received for publication, August 1, 2002, and in revised form, August 26, 2002
Published, JBC Papers in Press, August 27, 2002, DOI 10.1074/jbc.M207821200

Nils Hoffmann‡§, Amro A. Amara‡§, Br. Bernd Beermann¶, Qingsheng Qi‡, Hans-Jürgen Hinz¶, and Bernd H. A. Rehm‡‖

From the ‡Institut für Mikrobiologie der Westfälischen Wilhelms-Universität Münster, Corrensstrasse 3, D-48149 Münster, Germany and the ¶Institut für Physikalische Chemie der Westfälischen Wilhelms-Universität Münster, Schloßplatz 3, 48149 Münster, Germany

The 3-hydroxyacyl ACP:CoA transacylase (PhaG) was recently identified in various *Pseudomonas* species and catalyzes the diversion of ACP thioester intermediates of fatty acid *de novo* biosynthesis toward the respective CoA thioesters, which serve as precursors for polyester and rhamnolipid biosynthesis. PhaG from *Pseudomonas putida* was overproduced in *Escherichia coli* as a C-terminal hexahistidine-tagged (His_6) fusion protein in high yield. The His_6-PhaG was purified to homogeneity by refolding of PhaG obtained from inclusion bodies, and a new enzyme assay was established. Kinetic analysis of the 3-hydroxyacyl transfer to ACP, catalyzed by His_6-PhaG, gave $K_{0.5}$ values of 28 μM (ACP) and 65 μM (3-hydroxyacyl-CoA) considering V_{max} values of 11.7 milliunits/mg and 12.4 milliunits/mg, respectively. A Hill coefficient of 1.38 (ACP) and 1.32 (3-hydroxyacyl-CoA) indicated a positive substrate cooperativity. Subcellular localization studies showed that PhaG is not attached to polyester granules and resides in the cytosol. Gel filtration chromatography analysis in combination with light scattering analysis indicated substrate-induced dimerization of the transacylase. A threading model of PhaG was developed based on the homology to an epoxide hydrolase (1cqz). In addition, the alignment with the α/β-hydrolase fold region indicated that PhaG belongs to α/β-hydrolase superfamily. Accordingly, CD analysis suggested a secondary structure composition of 29% α-helix, 22% β-sheet, 18% β-turn, and 31% random coil. Site-specific mutagenesis of seven highly conserved amino acid residues (Asp-60, Ser-102, His-177, Asp-182, His-192, Asp-223, His-251) was used to validate the protein model and to investigate organization of the transacylase active site. Only the D182(A/E) mutation was permissive with about 30% specific activity of the wild type enzyme. Furthermore, this mutation caused a change in substrate specificity, indicating a functional role in substrate binding. The serine-specific agent phenylmethylsulfonyl fluoride (PMSF) or the histidine-specific agent diethylpyrocarbonate (DEPC) caused inhibition of 3-hydroxyacyl transfer to holo-ACP, and the S102(A/T) or H251(A/R) PhaG mutant was incapable of catalyzing 3-hydroxyacyl transfer, suggesting that these residues are part of a catalytic triad.

The transacylase $PhaG_{Pp}$ from *Pseudomonas putida* was the first enzyme identified and characterized to catalyze the reversible transfer of the (*R*)-3-hydroxydecanoyl moiety from the ACP thioester to CoA (1). This *in vivo* direction of the acyl transfer, *i.e.* the transfer of the acyl moiety from the ACP[1] thioester to CoA, has not been described for any other type of transacylase. $PhaG_{Pp}$ directly links the fatty acid *de novo* biosynthesis with the polyester (polyhydroxyalkanoate, PHA) biosynthesis by the provision of the activated precursor (*R*)-3-hydroxyacyl-CoA (Fig. 1). Meanwhile, these transacylases have also been found in other pseudomonads, which are capable of synthesizing medium-chain length polyester from non-related carbon sources (2–4). So far these enzymes have only been identified in bacteria belonging to pseudomonads also considering ongoing genome sequencing projects. The transacylase-mediated biosynthesis pathway has been already established in bacteria, which are not capable of accumulating polyester, by co-expression of a PHA synthase gene with the *phaG* gene (5, 6). PhaG exhibits a key enzyme activity in polyester production from non-related carbon sources, *i.e.* when the fatty acid *de novo* biosynthesis provides precursor and thus provides an important tool to establish this pathway in biotechnologically relevant organisms (6). In the primary structure of the transacylase, an HX_4D motif has been identified, which is conserved among glycosyltransferases (1). However, in the active transacylase found in *Pseudomonas* sp. 61-3 the Asp residue was replaced by a Leu residue, which indicated that this motif might not be required for enzyme activity. Meanwhile, nine *phaG* genes have been identified in nine *Pseudomonas* species, and four of the genes were functionally assigned (1–4). Interestingly, these transacylases share a rather high homology ranging from 75–98% similarity.

The aims of this study were: (i) the purification of the transacylase from *P. putida* at high yield, (ii) the establishment of a new enzyme assay, (iii) the enzymological and biochemical characterization of the enzyme, and (iv) the investigation of the catalytic mechanism.

EXPERIMENTAL PROCEDURES

Strains, Plasmids, and Cultivation Conditions—All bacteria and plasmids investigated in this study are listed in Table I. Cultivations were performed in Luria Bertani Broth (LB) or M9 medium containing the indicated carbon source, supplements, and antibiotics. Organic

* This study was supported by Grant Re 1097/4-1 from the Deutsche Forschungsgemeinschaft (to B. R.). The costs of publication of this article were defrayed in part by the payment of page charges. This article must therefore be hereby marked "*advertisement*" in accordance with 18 U.S.C. Section 1734 solely to indicate this fact.

§ Both authors contributed equally to this study.
‖ To whom correspondence should be addressed. Tel.: 49-251-8339848; Fax: 49-251-8338388; E-mail: rehm@uni-muenster.de.

[1] The abbreviations used are: ACP, acyl carrier protein; BSA, bovine serum albumin; NTA, nitrilotriacetic acid; PHA, polyhydroxyalkanoate; GC/MS, gas chromatography/mass spectrometry; DEPC, diethylpyrocarbonate; MRE, mean residue ellipticity; HPLC, high performance liquid chromatography; PMSF, phenylmethylsulfonyl fluoride.

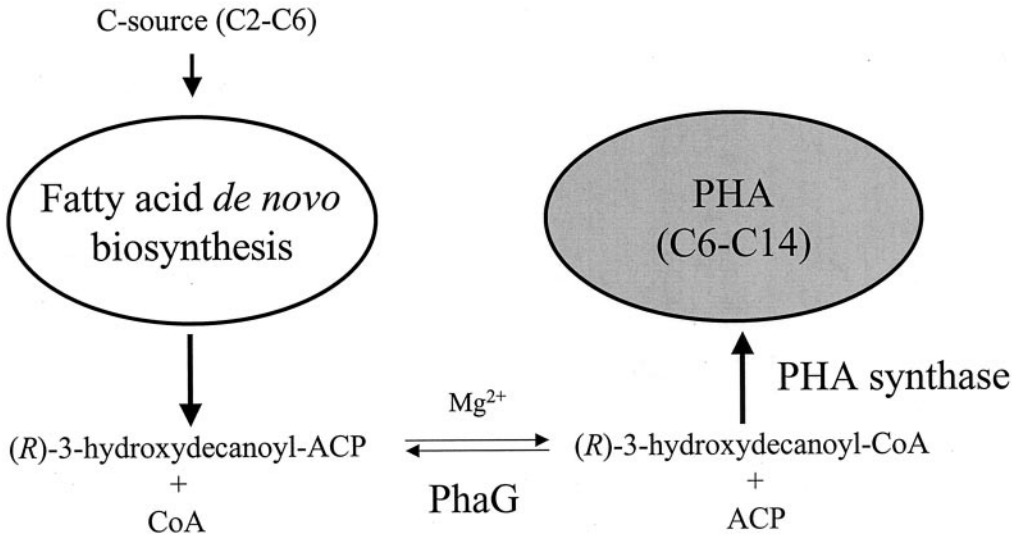

FIG. 1. **Reaction catalyzed by PhaG.**

acids were provided as sodium salts. Cultivations were conducted at 37 and 30 °C employing *E. coli* or *P. putida*, respectively, either with 50 ml of medium in 300-ml Erlenmeyer flasks that were agitated on a shaker at 200 rpm.

Isolation, Manipulation, and Mutagenesis of DNA—All genetic techniques were performed as described by Sambrook *et al.* (10). Site-specific mutagenesis of the various amino acid residues in the *P. putida* transacylase and the hexahistidine tag fusions of the transacylase were obtained employing overlapping PCR (11) and pBHR81 containing the 1-kb *Eco*RI-*Bam*HI fragment comprising the *phaG* gene from *P. putida* as template DNA (1). All oligonucleotides are summarized in Table I. Site-specific mutagenesis was conducted to replace seven amino acid residues, which were conserved among transacylases from pseudomonads. Mutagenized PCR products as well as PCR products encoding a C- or N-terminal His_6 tag were subcloned into *Eco*RI/*Bam*HI sites of plasmid pBBR1MCS-2 (8) directly downstream of the *lac* promoter in order to monitor the *in vivo* activity of the respective transacylase. For the construction of *phaG*-overexpressing plasmids, the coding region of the *phaG* gene from *P. putida* was amplified by tailored PCR introducing restriction sites for *Nde*I and *Bam*HI at the 5′- and 3′-end, respectively. The resulting PCR product was inserted into the corresponding restriction sites of vector pT7-7, resulting in plasmid pAM1, under the control of T7 RNA polymerase promoter Ø10. *E. coli* BL21(DE3) was used to overexpress the gene encoding the His_6-tagged fusion protein.

Isolation and Purification of Inclusion Bodies—Cells were dissolved in 50 mM phosphate buffer, pH 8.0, containing lysozyme and DNase I and incubated on ice for 30 min. Then EDTA was added to a final concentration of 10 mM, and the cells were incubated on ice for another 20 min. After French press treatment, the crude extract was centrifuged at 10,000 × *g* for 20 min to obtain the insoluble fraction. The resulting sediment was suspended in 50 mM phosphate buffer, pH 8.0, containing 0.15 M NaCl and 1 mM EDTA. After incubation on ice for 20 min, the inclusion bodies were sedimented as described above. The inclusion bodies were washed in phosphate buffer containing 2 M urea and 0.5% Triton X-100. Finally the purified inclusion bodies were dissolved in phosphate buffer containing 6 M guanidine HCl and 3 mM 2-mercaptoethanol. The guanidium HCl insoluble materials were removed by centrifugation at 10,000 × *g* for 10 min.

Purification and Refolding of PhaG—The dissolved and denatured protein was subjected to metal chelate affinity chromatography using a Ni^{2+}-NTA acid resin (Qiagen, Germany) with a bed volume of 5 ml. Equilibration was performed according to the manufacturer's protocol on an FPLC apparatus (Amersham Biosciences) with 50 mM phosphate buffer, pH 8.0, containing 300 mM NaCl, 8 M urea, 1 mM 2-mercaptoethanol, and 10% glycerol. After washing at pH 6.3, the denatured His-tagged PhaG was eluted at pH 4.3. Refolding was achieved by applying purified and denatured His-tagged PhaG, whose concentration was adjusted to 50 μg/ml to gel filtration chromatography using Sephadex G25. This column was equilibrated with 20 mM phosphate buffer, pH 8.0, and the refolded active enzyme was obtained after elution.

Purification of His_6-PhaG under Native Conditions—His_6-PhaG was purified under native conditions using native PAGE as previously described (1).

Analytical Gel Filtration Chromatography—The native molecular mass of the refolded PhaG was estimated by gel filtration chromatography on Superdex 200 HR 10/30 column (10 × 300 mm) equilibrated with 50 mM sodium phosphate buffer (pH 7.0) containing 0.15 M NaCl and at a flow rate of 1 ml/min. The analyzed protein sample was directly taken from the refolding experiment, applying 4 ml with about 30 μg/ml protein concentration. Protein in the eluate was monitored at A_{280}; fractions were collected and analyzed by SDS-PAGE. For calibration, standard proteins (Amersham Biosciences) were chromatographed under the same conditions.

Dynamic Light Scattering (DLS)—All light scattering experiments were performed with a DynaPro molecular sizing instrument (Protein Solutions) at a fixed angle of 90°. The Dynamics 5.25.44 software package was used for data analysis. The translational diffusion coefficient (D_T) of the sample particles was determined by measuring the fluctuations in the intensity of scattered light with an autocorrelation function. The hydrodynamic radius (R_h) of the particles was calculated by the Stokes-Einstein equation ($D_T = k_B T/6\pi\eta R_h$, with k_B referring to Boltzmann's constant, T to the absolute temperature, and η to the solvent viscosity). Assuming that the particles are spherical and of standard density, the molecular mass of the particles was estimated from R_h. The autocorrelation function was analyzed using a bimodal exponential cumulant analysis procedure. The polydispersity parameter and the error distribution function provided evidence of the homogeneity of the particle size in the solution. Before the DLS experiments all protein solutions were filtered using a 0.02-μm filter (Anodisc 13; Whatman). DLS of refolded transacylase was measured at 25 °C and at a concentration of 0.55 mg ml^{-1} in 10 mM sodium phosphate buffer (pH 8.0); 50 independent measurements were accumulated for each sample, and the values reported are the mean values.

Circular Dichroism Spectroscopy—CD spectra were recorded on a Jobin-Yvon (Paris) spectropolarimeter, model CD 6′, equipped with a self constructed cuvette holder whose temperature is controlled by a Peltier element. Measurements were performed in 10 mM sodium borate buffer (pH 9.0) or 10 mM sodium phosphate buffer (pH 8.0). The spectra were recorded at 20 °C. The protein concentrations used ranged from 390 to 590 μg/ml. A cuvette of 0.1-mm path length was used. The results were expressed as mean residue ellipticity, $[\Theta]_{MRE} = (MRW \cdot \theta_{obs}/c \cdot d)$, where θ_{obs} is the observed ellipticity, MRW is the mean residue weight of PhaG fusion protein (106,72 Da), d is the cuvette path length, and c is the specific protein concentration. Deconvolution of CD spectra was done using the program CDNN of Bohm *et al.* (12).

SDS PAGE and Western Immunoblotting—SDS-PAGE was performed according to Sambrook *et al.* (10). Proteins were separated in 12.5 (w/v) % SDS-polyacrylamide gels and stained with Coomassie Brilliant Blue R-250. Western blotting was performed using the Semidry Fastblott (Biometra, Germany). On Western blots (13) using nitrocellulose membranes the PHA synthase and its mutants were detected applying the respective monospecific, polyclonal anti-PhaG antiserum raised against the PhaG from *P. putida* and an alkaline-phosphatase-

TABLE I
Bacterial strains, plasmids and oligonucleotides

Strains, plasmids and oligonucleotides	Relevant characteristics	Source or reference
Escherichia coli		
XL1-Blue	*rec*A1 *end*A1 *gyr*A96 *thi hsd*R17 (r_K^-,m_K^+) *sup*E44 *rel*A1 λ^- *lac* [F′ *proAB lacI*^{q} *lacZ*ΔM15 Tn*10*(*Tc*^{r})]	(7)
BL21 Star™ (DE3)	F′ *ompT hsdS*$_B$ ($r_B^-m_B^-$) *gal dcm rne131* (DE3)	Invitrogen
Pseudomonas putida		
PHAG$_N$-21	*P. putida* KT2440 mutant	(1)
Plasmids:		
pBBR1MCS-2	Km^r, broad host range, *lac*POZ′	(8)
pT7–7	Ap^r, T7 RNA polymerase promoter	(9)
pBHR81	pBBR1MCS-2 containing coding region of *phaG* in *Eco*RI/*Bam*HI site downstream of *lac* promotor	(1)
pQQ19	pBHR81 encoding N-terminal His6-tagged PhaG	This study
pQQ20	pBHR81 encoding C-terminal His6-tagged PhaG	This study
pNH1-D60A	pBHR81 with site-specific mutation in *phaG* gene causing D60A replacement	This study
pNH2-D60E	see pNH1-D60A	This study
pNH3-S102A	see pNH1-D60A	This study
pNH4-S102T	see pNH1-D60A	This study
pNH5-H177A	see pNH1-D60A	This study
pNH6-H177R	see pNH1-D60A	This study
pNH7-D182A	see pNH1-D60A	This study
pNH8-D182E	see pNH1-D60A	This study
pNH9-H192A	see pNH1-D60A	This study
pNH10-H192R	see pNH1-D60A	This study
pNH11-D223A	see pNH1-D60A	This study
pNH12-D223E	see pNH1-D60A	This study
pNH13-H251A	see pNH1-D60A	This study
pNH14-H251R	see pNH1-D60A	This study
pAA1	pT7–7 containing C terminal his$_6$-tag *phaG* in *Nde*I/*Bam*HI site downstream of T7 RNA polymerase promotor	This study
pNH15-D60A	pAA1 with site-specific mutation in *phaG* gene causing D60A	This study
pNH16-D60E	see pNH15-D60A	This study
pNH17-S102A	see pNH15-D60A	This study
pNH18-S102T	see pNH15-D60A	This study
pNH19-H177A	see pNH15-D60A	This study
pNH20-H177R	see pNH15-D60A	This study
pNH21-D182A	see pNH15-D60A	This study
pNH22-D182E	see pNH15-D60A	This study
pNH23-H192A	see pNH15-D60A	This study
pNH24-H192R	see pNH15-D60A	This study
pNH25-D223A	see pNH15-D60A	This study
pNH26-D223E	see pNH15-D60A	This study
pNH27-H251A	see pNH15-D60A	This study
pNH28-H251R	see pNH15-D60A	This study
Oligonucleotides:		
For amplification of *phaG*		
5′ end	5′-CGGAATTCAAGGAGTCGATGACATG-3′	
3′ end	5′-CGCGGATCCCGGCGCCCCGTGGCC-3′	
For site-specific mutagenesis		
D60A	5′-CCTGAATACGGCTGAGCGAACAGAACCACG-3′	
D60E	5′-CCTGAATACGGCTGCTCGAACAGAACCACG-3′	
S102A	5′-CTTGCGCCACCCCAAGCAAAAGACATCACG-3′	
S102T	5′-CTTGCGCCACCCCACGTAAAAGACATCACG-3′	
H177A	5′-TCCAGGCTGCTCACAGCGCGGTAGTTGAAG-3′	
H177R	5′-TCCAGGCTGCTCACGCGGCGGTAGTTGAAG-3′	
D182A	5′-CGCTACTCGTGGCTAGCCAGGCTGCTCACA-3′	
D182E	5′-GCGTACTCGTGGCTCTCCAGGCTGCTCACA-3′	
H192A	5′-AGCACCTGGTTGATAGCGAAGTGCATCTGT-3′	
H192R	5′-AGCACCTGGTTGATGCGGAAGTGCATCTGT-3′	
D223A	5′-ACTGTGGTGTACTCCTCGCGCTCGCCGTTG-3′	
D223E	5′-ACTGTGGTGTACTCCTCGCGCTCGCCGTTG-3′	
H251A	5′-TCCATGTCCAGGAAAGCGCCCGCATCGCGG-3′	
H251R	5′-TCCATGTCCAGGAAGCGGCCCGCATCGCGG-3′	
For construction of genes encoding His$_6$-tagged fusion proteins		
N terminus		
5′-end	5′-GGGAATTCCATATGAGGCCAGAAATCGCTGTACTTG-3′	
3′-end (His$_6$)	5′-CGGGATCCTCAGTAGTGGTAGTGGTAGTGGATGGCAAATGCATGCTGCCC-3′	
C terminus		

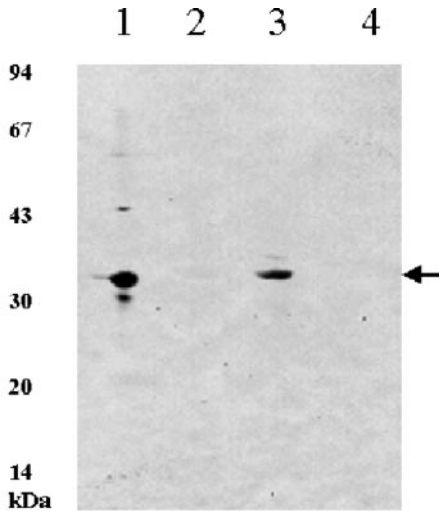

FIG. 2. **Subcellular localization of PhaG by Western immunoblotting.** *Lanes*: *1*, purified PhaG inclusion bodies (positive control); *2*, crude extract from *P. oleovorans* (negative control); *3*, cytosolic fraction from *P. putida*; *4*, envelope and PHA-granule fraction from *P. putida*. Monospecific anti-PhaG antibodies were applied. The *arrow* indicates the position of PhaG.

antibody conjugate as second antibody. Bound antibodies were detected using the luminogenic substrate CDP-Star (Amersham Biosciences) and exposure to x-ray film.

In Vivo Activity of the Transacylase—In vivo activity of the respective transacylase was obtained by complementation of *phaG*-negative mutant *P. putida* $PhaG_N$-21 (1). Recombinant cells harboring the respective plasmid were cultivated in MM medium plus 1.5% (w/v) sodium gluconate, and after 48 h incubation at 30 °C the PHA content of lyophilized cells was determined by GC analysis. PHA accumulation from gluconate indicated *in vivo* activity of PhaG. The activity of modified transacylases was obtained relative to the wild type transacylase activity, *i.e.* as the amount of accumulated PHA mediated by the wild type enzyme.

In Vitro Activity of the Transacylase—PhaG activity was determined spectrophotometrically by monitoring the release of CoA using the thiol reagent 5,5′-dithionitrobenzoic acid (DTNB) and measuring the change in absorbance at 412 nm. The standard assay contained 3 mM $MgCl_2$, 40 μM of the respective CoA thioester and 20 μM holo-ACP in 50 mM Tris/HCl, pH 7.5, at 30 °C in a total volume of 100 μl. Kinetic studies were performed by removing aliquots (10 μl) from the reaction mixture at timed intervals, and the reaction was stopped by addition of 50% (w/v) trichloroacetic acid (30 μl) and 10 mg/ml BSA (30 μl). BSA was added as a carrier (30 μl, 10 mg/ml), and the protein (PhaG and ACP) was allowed to precipitate on ice for 15 min and then pelleted by centrifugation. Released CoA was spectrophotometrically determined employing the thiol reagent DTNB as previously described (1). One unit of enzyme has been defined as the amount which produced 1 μmol of acyl-ACP (1 μmol of released CoA) per minute under the assay conditions employed. All assays were repeated in triplicate, and appropriate control experiments were routinely performed.

Inhibition Studies Using PMSF—His_6-PhaG (1 mM) was incubated in 50 mM phosphate buffer (pH 7.5) for 60 min at 30 °C with 0, 0.1, 1, and 2 mM PMSF in a total volume of 100 μl. Aliquots were removed to determine the CoA release as described above. To assess the ability of 3-hydroxydecanoyl-CoA to protect the enzyme from inhibition, 1 mM His_6-PhaG was incubated for 5 min at 30 °C with 100 and 500 μM 3-hydroxydecanoyl-CoA, respectively. The aliquots were diluted to volumes of 20 μl by addition of PMSF in buffer to the appropriate concentrations, and the inhibition experiments were repeated.

Inhibition Studies Using DEPC—For inhibition studies, 1 mM purified PhaG was incubated at 30 °C in 40 mM potassium phosphate, pH 7.5, with various concentrations of the histidine reagent DEPC (Sigma) for 60 min. DEPC solutions (in ethanol) were made each day just prior to an experiment. Exact DEPC concentrations were determined by reacting with an excess of imidazole (Sigma) and measuring the A_{240} ($\epsilon = 3200\ M^{-1}$) (14). DEPC reactions with PhaG at 30 °C were quenched by a 1:50 dilution into 10 mM imidazole (on ice) (at least a 10-fold molar excess over the DEPC). DEPC, ethanol, and imidazole at the concentrations used have no effect on the substrates of the PhaG reaction, and ethanol and imidazole have no effect on PhaG activity at the levels at which they are carried over into the assay mixture (not shown). The PhaG/DEPC/imidazole mixtures were further diluted with 1 mg/ml BSA and assayed by the standard method as described above. For substrate protection studies, 1 mM purified PhaG was incubated at 30 °C for 5 min in 40 mM potassium phosphate, pH 7.5, and 2 mM DEPC in the presence of 100 and 500 μM 3-hydroxydecanoyl-CoA. The reactions were quenched by a 1:50 dilution into 10 mM imidazole. The mixtures were then further diluted as appropriate into 1 mg/ml BSA and assayed by the standard method as described above.

TABLE II

In vivo activity of various His_6 tag fusions of the transacylase PhaG

Cultivations were performed under PHA-accumulating conditions on mineral salt medium containing 1.5% (w/v) sodium gluconate and 0.05% (w/v) ammonium chloride. Cells were grown for 48 h at 30 °C. PHA content, and composition of comonomers were analyzed by GC/MS.

Strain and plasmid	PHA content	Relative *in vivo* transacylase activity
	(% (w/w), CDW)	%
P. putida $PHAG_N$-21 (pBBR1MCS-2)	1.7	0
P. putida $PHAG_N$-21 (pQQ19/N-terminal His_6 tag)	4.3	6.8
P. putida $PHAG_N$-21 (pQQ20/C-terminal His_6 tag)	36.7	91
P. putida $PHAG_N$-21 (pBHR81/wild type)	40.1	100

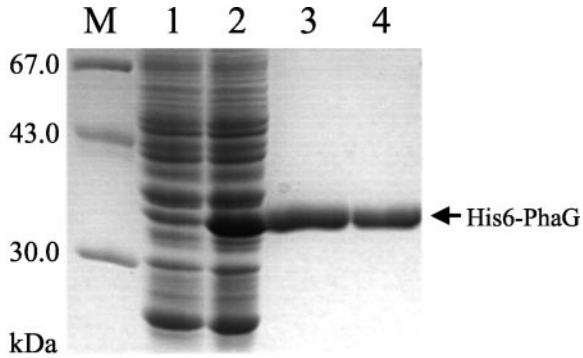

FIG. 3. **SDS-PAGE analysis of the overproduced, refolded, and purified PhaG fusion protein.** *Lane M*, molecular weight standard; *lane 1*, crude extract of *E. coli* BL21(DE3) harboring pT7-7 (negative control); *lane 2*, crude extract of *E. coli* BL21(DE3) harboring pAA1 (positive control); *lane 3*, purified inclusion bodies from *E. coli* BL21(DE3) harboring pAA1; *lane 4*, purified and refolded His_6 tag PhaG.

Gas Chromatographic/Mass Spectrometry Analysis of Polyester in Cells—PHA was qualitatively and quantitatively analyzed by gas chromatography/mass spectrometry (GC/MS). Liquid cultures were centrifuged at 10,000 × *g* for 15 min, then the cells were washed twice in saline and lyophilized overnight. 8–10 mg lyophilized cell material was subjected to methanolysis in the presence of 15% (v/v) sulfuric acid. The resulting methyl esters of the constituent 3-hydroxyalkanoic acids were assayed by GC/MS according to Brandl *et al.* (15) and as described in detail previously (16). GC/MS analysis was performed by injecting 3 μl of sample into a PerkinElmer 8420 gas chromatograph (Überlingen, Germany) using a 0.5-μm-diameter Permphase PEG 25 Mx capillary column 60 m in length.

Analysis of (R,S)-3-Hydroxydecanoyl-CoA—The substrate (*R,S*)-3-hydroxydecanoyl-CoA was synthesized as previously described (1). (*R,S*)-3-hydroxydecanoyl-CoA was purified using Sep-Pak cartridges (reversed-phase C_{18} column, Waters) and eluting the CoA thioester with 0.01 N NaOH in 20% (v/v) methanol. The purified (*R,S*)-3-hydroxydecanoyl-CoA was analyzed by HPLC, and its concentration was determined by hydroxylamine treatment, which causes a release of bound CoA. The concentration of free CoA before and after hydroxylamine treatment (17) was analyzed by the Ellman method (18).

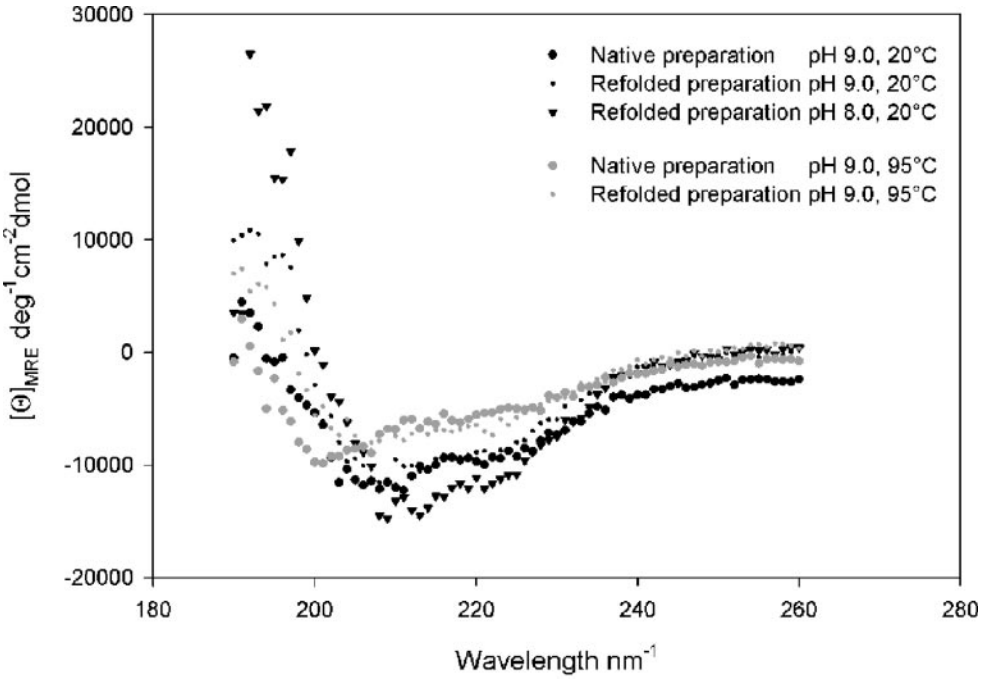

FIG. 4. **CD spectroscopic analysis of native, refolded, and heat denatured (95 °C) PHA transacylase fusion protein.** Spectra were recorded from 195 to 260 nm. The proteins were measured at temperatures indicated in the graph. Buffer conditions: 10 mM sodium borate solution, pH 9.0; or 10 mM sodium phosphate buffer, pH 8.0. Protein concentrations: native protein: 390 μg/ml; refolded PhaG fusion protein: 550–590 μg/ml. Protein solutions were measured in a 0.1-mm cuvette. All spectra were recorded ten times and averaged. Integration time was 1 s per data point.

RESULTS

Subcellular Localization of PhaG in P. putida—Since various enzymes involved in PHA biosynthesis are localized at the PHA-granule surface, we investigated the subcellular localization of PhaG in *P. putida*. Therefore, *P. putida* cells were cultivated under PHA accumulation conditions employing nitrogen-starvation and gluconate as sole carbon source. The soluble cytosolic fraction and the insoluble envelope/PHA-granule fraction were obtained by ultracentrifugation of crude extracts. PhaG was only detected in the soluble cytosolic fraction by immunoblotting applying monospecific anti-PhaG-antibodies raised against PhaG from *P. putida* (Fig. 2).

Overproduction of PhaG—The expression of the transacylase gene *phaG* under control of the *lac* promoter was weak and resulted only in a PhaG production of about 5% total protein (1). In this study, we have subcloned the *P. putida phaG* into the *E. coli* expression vector pT7-7 as described under "Experimental Procedures," allowing PhaG to be overproduced as a His_6-tagged protein with *phaG* under Ø10 promoter control. Since, the N-terminal His tag fusion showed only 6.8% of wild type activity and the C-terminal His tag fusion exhibited 91% of wild type activity, the C-terminal His_6 tag fusion was overproduced (Table II). The respective plasmid pAM1, which contained the coding region encoding the His_6 tag fusion protein collinear to the Ø10 promoter in restriction sites *Nde*I and *Bam*HI, was transferred into *E. coli* BL21(DE3) and, upon induction of the T7 RNA polymerase gene with 1 mM isopropylthio-β-D-galactoside, overproduction of the His_6 tag fusion protein was observed, amounting to about 80% of the total protein (Fig. 3). The His_6 tag fusion protein occurred as inactive inclusion bodies. This was concluded from microscopic observations of light-scattering inclusions in cells as well as from the isolated insoluble fusion protein. No *in vivo* activity of the overproduced fusion protein was obtained, which was concluded from the absence of PHA accumulation in recombinant *E. coli* as described previously (6). For the test gluconate was provided as carbon source, and the fatty acid *de novo* biosynthesis was inhibited with triclosan, in order to provide substrates for class II PHA synthases mediated by PhaG. Enzymatic activity correlates with the accumulation of PHA, which can be determined by GC/MS analysis. Cells overproducing the fusion protein did not show any accumulation of PHA. Moreover, no *in vitro* enzymatic activity was detected.

Purification of PhaG from Inclusion Bodies—Inclusion bodies from *E. coli* BL21(DE3) harboring pAA1 of a 100-ml culture were isolated and purified as described under "Experimental Procedures." After the final washing of the inclusion bodies a purity of transacylase fusion protein of about 80% was obtained (Fig. 3). *E. coli* crude extracts containing the inclusion bodies and purified inclusion bodies were each subjected separately to *in vitro* enzymatic activity analysis using (*R,S*)-3-hydroxydecanoyl-CoA as substrate and holo-ACP as acceptor, but no enzymatic activity was detected, respectively. The purified inclusion bodies were dissolved in 6 M guanidium-HCl and 3 mM 2-mercaptoethanol. The denatured PhaG fusion protein was then purified to electrophoretic homogeneity by metal chelate affinity chromatography and was refolded by gel filtration chromatography as described under "Experimental Procedures." The PhaG-containing fraction was collected and subjected to SDS-PAGE analysis. SDS-PAGE analysis showed that the PhaG fusion protein was purified to homogeneity (Fig. 3). The purified and refolded His_6 tag PhaG was analyzed for *in vitro* enzyme activity. A specific enzyme activity of 12.4 milliunits/mg protein was determined using (*R*)-3-hydroxydecanoyl-CoA as substrate.

CD Spectroscopy of Transacylase—In order to provide further evidence for proper refolding of the transacylase fusion protein, CD spectroscopy was employed. Both native and refolded protein, purified as described above, was used for the measurements. To allow comparison of the secondary structure content of the native, refolded and denatured protein, CD spectra of all three species were recorded under the same buffer conditions. The CD spectra of native and refolded protein are evidently similar at pH 9.0 and 20 °C (Fig. 4). The spectra of both purified native and refolded protein show characteristic minima at 208 and 222 nm, indicative of α-helical structure.

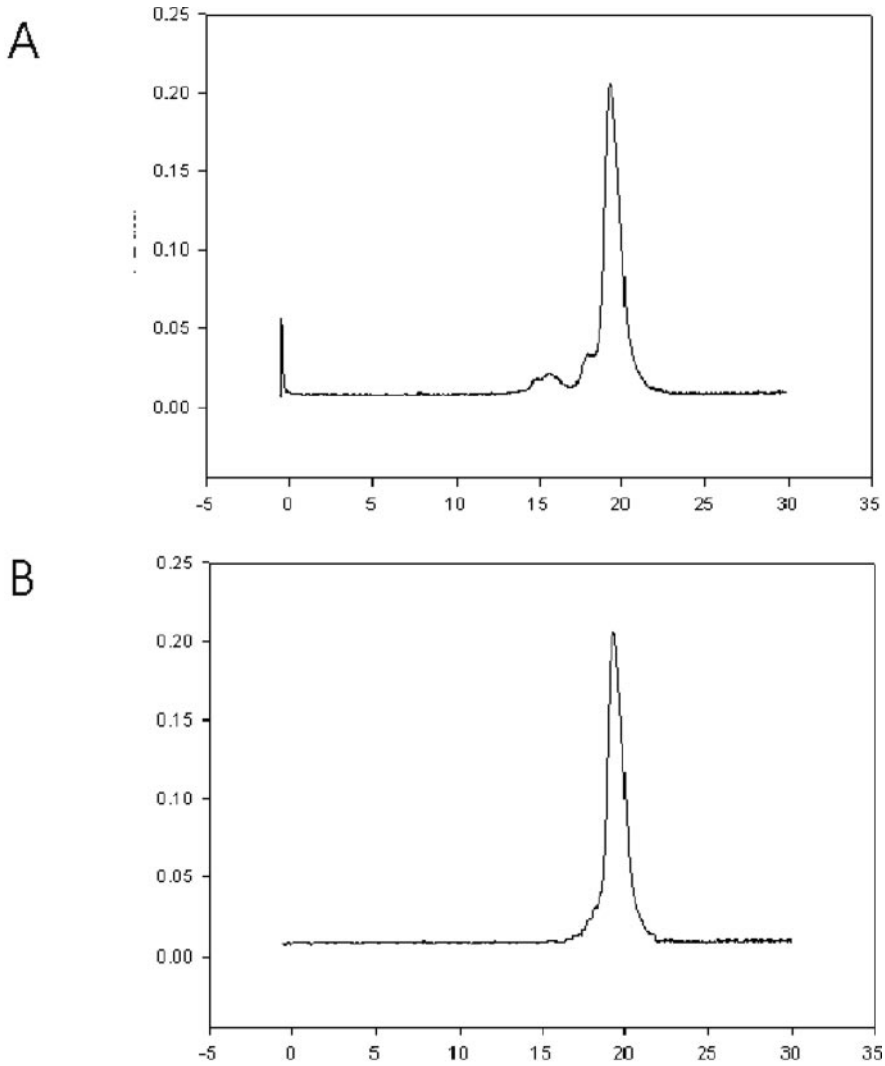

FIG. 5. **Gel filtration chromatography analysis of PhaG, in the absence of (*R*)-3-hydroxydecanoyl-CoA (*A*) and in the presence of (*R*)-3-hydroxydecanoyl-CoA (*B*).**

However, the absolute MRE values suggest a relatively low α-helical content. Therefore other conformational motifs such as β-sheets and coiled elements appear to determine the structure. This interpretation is supported by the deconvolution of the spectra, which resulted in the following secondary structure composition: 28% α-helices, 24% β-sheet, 18.5% β-turn, and 30% random coil. The spectrum of the denatured protein at 95 °C shows the typical random coil ellipticity.

When decreasing the pH from 9.0 to 8.0 at 25 °C a significant change toward negative MRE values is observed. This is indicative of a more native-like structure at a pH value closer to physiological conditions.

Analysis of the Molecular Weight of the Refolded His_6-PhaG—In order to analyze the molecular weight of the active and refolded His_6-PhaG from *P. putida*, we performed gel filtration chromatography as well as light-scattering analysis. His_6-PhaG obtained after refolding at a protein concentration of about 0.1 mg/ml was directly subjected to gel filtration chromatography applying Superdex 200. A single peak was obtained, which indicated an apparent molecular weight of 33,080, while the exact molecular weight of the His_6-tagged PhaG is 34,737 (Fig. 5). In the presence of the substrate (*R*)-3-hydroxydecanoyl-CoA additional peaks were observed corresponding to apparent molecular weights of 45.4, 83.7, and 102, respectively (Fig. 5). The refolded His_6-PhaG was concentrated by 10-fold applying ultrafiltration and resulting in a protein concentration of about 1 mg/ml. This sample was subjected to dynamic light scattering analysis, which indicated a molecular weight of about 68 (Fig. 6).

Establishment of an in Vitro Transacylase Assay—Purified and refolded His_6-PhaG was first assayed qualitatively for its ability to catalyze the transfer of 3-hydroxydecanoyl from 3-hydroxydecanoyl-CoA to *E. coli* holo-ACP, using HPLC analysis as previously described (1). A new enzyme assay was established allowing determination of PhaG activity spectrophotometrically by monitoring the release of CoA at 412 nm. Released CoA was spectrophotometrically determined employing the thiol reagent DTNB. The holo-ACP, whose thiol group would interfere with the detection of CoA, was removed by trichloroacetic acid precipitation. Kinetic studies were performed by removing aliquots (10 μl) from the reaction mixture at timed intervals as described under "Experimental Procedures."

Kinetic Analysis of PhaG—The turnover of 3-hydroxydecanoyl-CoA catalysed by PhaG was monitored as a function of time. The reaction was started applying *E. coli* holo-ACP. No lag phase was observed, and about 80% of the 3-hydroxydecanoyl-CoA was converted to 3-hydroxydecanoyl-ACP (Fig. 7). The formation of 3-hydroxydecanoyl-ACP was confirmed by HPLC analysis as previously described (1). The enzyme activity was recorded as a function of 3-hydroxydecanoyl-CoA and 3-hydroxydecanoyl-ACP concentration, respectively. A sigmoidal curve was obtained in both experiments, which could be represented as a Hill plot indicating that the transacylase behaves

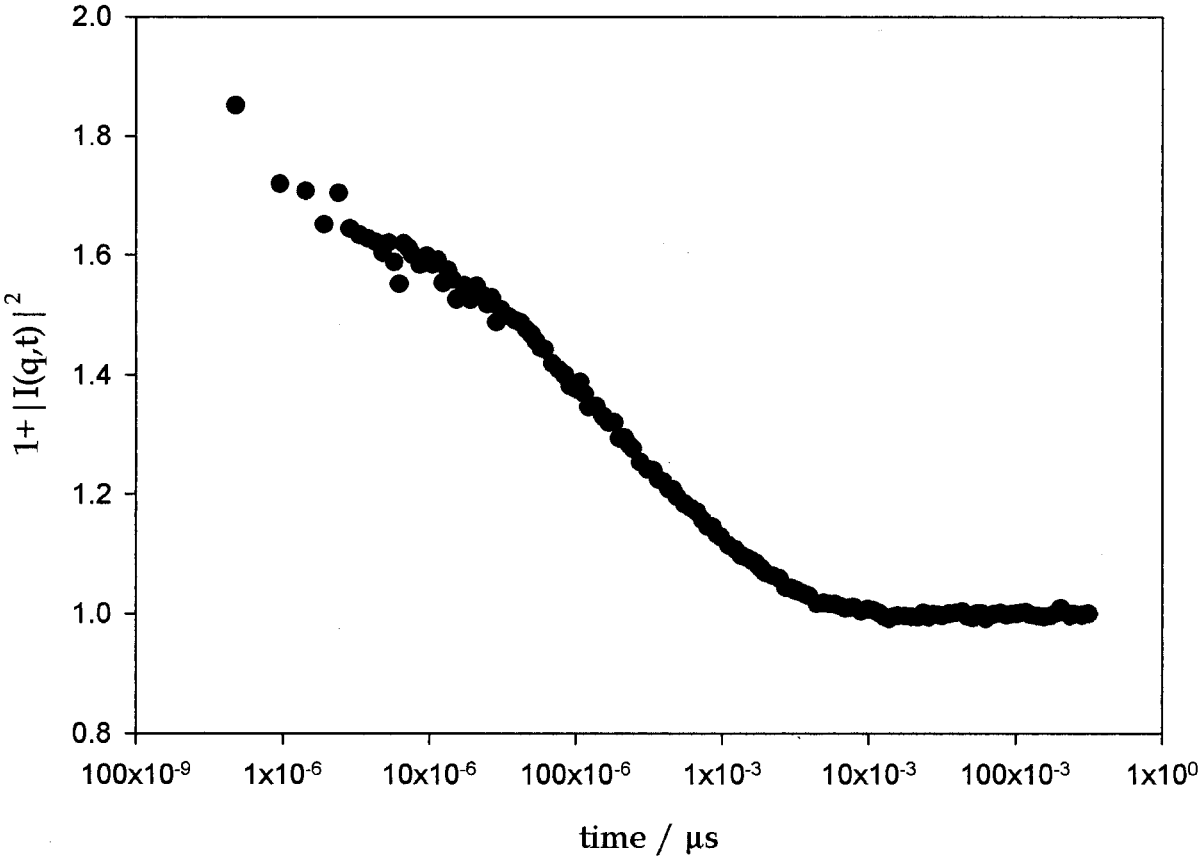

FIG. 6. **Autocorrelation function of PHA transacylase (c, 0.55 mg ml^{-1}) measured by dynamic light scattering at 25 °C in 10 mM sodium phosphate buffer (pH 8.0).** Each point of the curve represents the mean of 50 measurements.

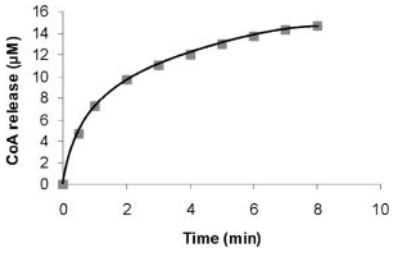

FIG. 7. **Time course of CoA release by His$_6$-tagged PhaG from 40 µM (*R*)-3-hydroxydecanoyl-CoA and 20 µM holo-ACP.** CoA release was monitored in a discontinuous assay using DTNB (Ellman, 1959). The transacylase was applied at a concentration of 10 µg/ml.

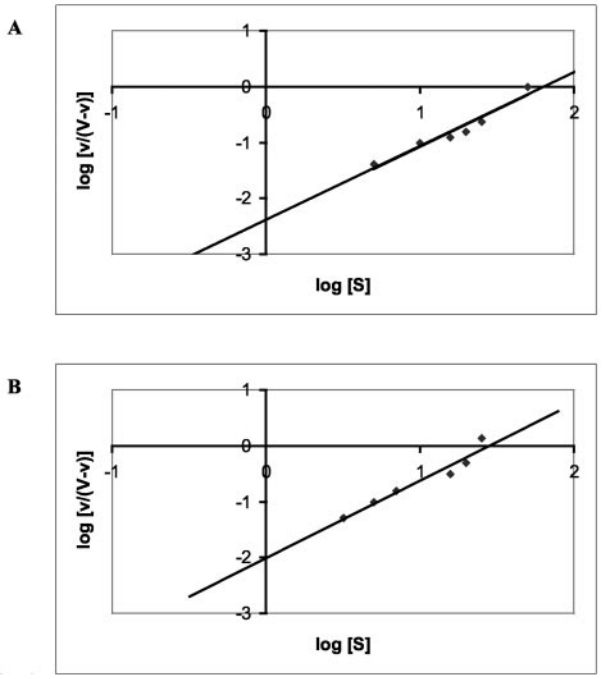

FIG. 8. ***In vitro* activity of His$_6$-tagged PhaG employing various concentrations of (*R*)-3-hydroxydecanoyl-CoA (*A*) and holo-ACP (*B*).** The transacylase was applied at a concentration of 10 µg/ml. Data are presented as Hill plots.

as an allosteric enzyme (Fig. 8). The Hill plot analysis revealed Hill coefficients of 1.32 and 1.38 for (*R*)-3-hydroxydecanoyl-CoA and holo-ACP, respectively, which indicated positive substrate cooperativity. $K_{0.5}$ values of 65 µM and 28 µM for (*R*)-3-hydroxydecanoyl-CoA and holo-ACP, respectively, were also obtained from Hill plot analysis. A V_{max} of 12.4 milliunits/mg and 11.7 milliunits/mg with (*R*)-3-hydroxydecanoyl-CoA and holo-ACP, respectively, was estimated from Lineweaver-Burk plot analysis considering substrate concentrations of >15 µM.

Development of a Threading Model of the P. putida Transacylase—A PSI-Blast search in combination with a conserved domain alignment showed about 30% similarity of PhaG with the epoxide hydrolase (1cqz) from mouse and about 22% identity with conserved α/β-hydrolase fold region (Fig. 9). These alignments were used to generate a threading model of PhaG (residues 7–285) including two small deletions (22–24, 260–262). Deletions were introduced, because no homology of these regions to structurally conserved regions was found, and the loop search against a loop fold library failed (Homology (software package), Molecular Simulations). However, deletions were located in variable regions according to the multiple alignment of transacylases (Fig. 10). A threading model of PhaG was finally

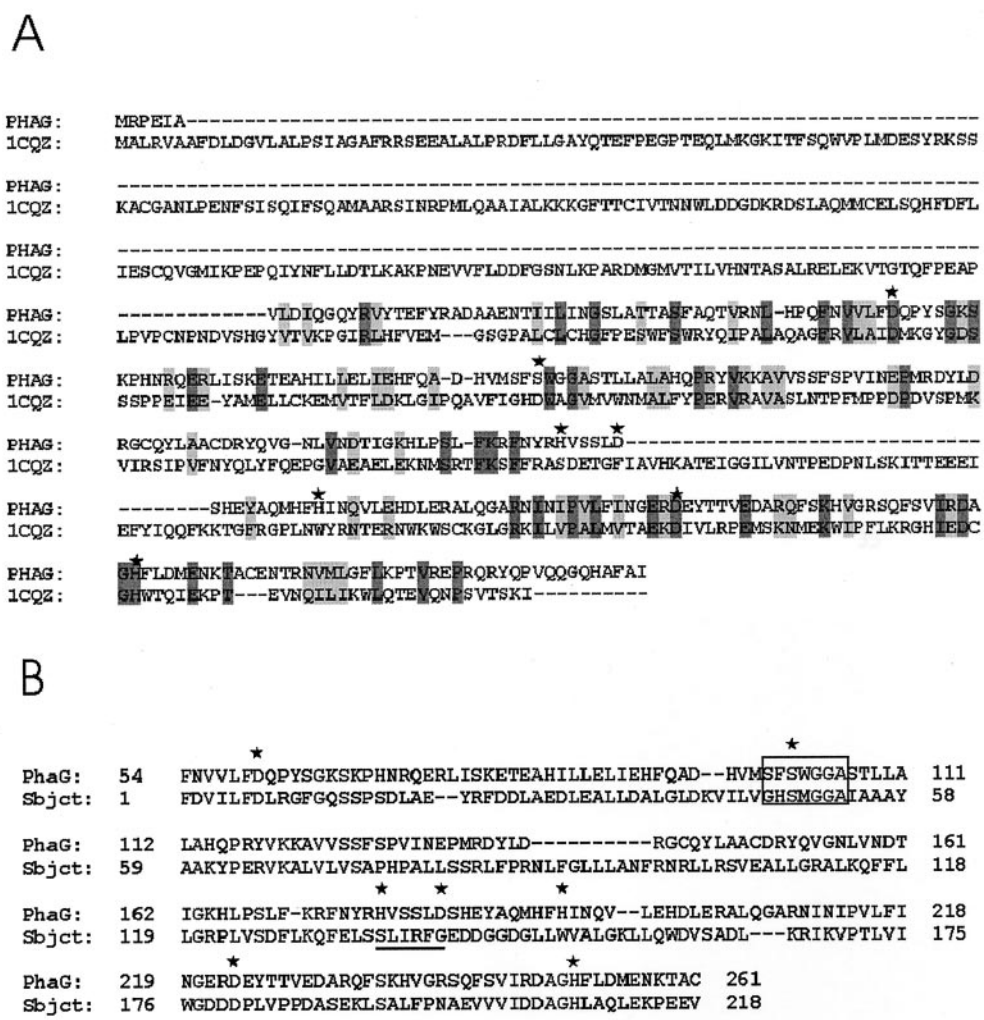

FIG. 9. **Alignment of the *Pseudomonas putida* transacylase PhaG with the *mouse* epoxide hydrolase (1cqz) (*A*) and the conserved *α/β*-hydrolase fold region (*B*).** The alignment was performed using PSI-Blast and the conserved domain (*CD*) search, respectively. Conservative replacements are labeled with a *light gray* background, and identical residues are labeled with *dark gray* background. Mutagenized residues are labeled with *asterisks*. The putative lipase-box is *underlined* or *boxed*.

developed using software packages Homology and Discover (Molecular Simulations) (Fig. 11). Energy minimization was performed employing the consistent valence force field (CVFF) implemented in DISCOVER. The stereochemistry of the model structure was evaluated with the program PROCHECK (19), and the residue environment was analyzed with the VERIFY_3D program that implements the algorithm of Lüthy *et al.* (20). The resulting model suggests that PhaG is a member of the superfamily of the α/β-hydrolases possessing a conserved α/β-hydrolase fold as the core structure. Additional submission of the PhaG sequence to three other algorithm that search structural databases (SAM-T98, Ref. 21; 3D-PSSM, Ref. 22; and the UCLA Foldserver, Ref. 23) resulted in fits to other enzymes belonging to the α/β-hydrolase fold family with high confidence levels (data not shown). Inspection of the protein model of PhaG showed that a putative active site Ser-102, a conserved His-251, and the Asp-223, presumably forming a catalytic triad, are adjacent to the core structure (Fig. 11). These residues are conserved in all transacylases. The putative active site Ser-102 was located at the nucleophile elbow, a sharp γ turn containing the nucleophilic residue, positioned between a β-strand and an α-helix, which is one of the most conserved features of the α/β-hydrolase enzymes. Moreover, Ser-102 is located in a "lipase-box (G*X*S*X*G)"-like pentapeptide SFSWG.

Active Site Residues—We probed the active site of *P. putida* PhaG by incubating it with the hydroxyl-specific agent PMSF. Preincubation of His_6-PhaG with PMSF caused significant inhibition (Table III). However, preincubation in the presence of the substrate, 3-hydroxydecanoyl-CoA, reduced the level of inhibition, indicating the likelihood of a nucleophilic hydroxyl at the active site. Furthermore, the histidine reagent DEPC was used to study the role of histidines in enzyme activity. Incubation of purified His_6-PhaG with DEPC, a histidine reagent, causes inhibition of enzymatic activity (Table III). His_6-PhaG is stable under the preincubation conditions in the absence of DEPC. The inhibition of activity depends upon the concentration of DEPC. To determine whether the inactivation of His_6-PhaG results from modification of an active site residue, we looked for substrate protection against DEPC inactivation. The substrate 3-hydroxydecanoyl-CoA protects His_6-PhaG from inactivation by DEPC (Table III). Holo-ACP itself contains one histidine residue, and consequently care was taken to ensure that holo-ACP was not simply scavenging the DEPC reagent. Protection by 3-hydroxyacyl-CoA suggests that the modified residue accounting for the inactivation is in the *P. putida* PhaG active site or at least in the cleft which docks 3-hydroxyacyl-CoA.

Mutational Analysis of the P. putida PhaG—With the aid of the multiple PhaG sequence alignment (ClustalW), we depicted seven amino acid residues (Asp-60, Ser-102, His-177, Asp-182,

FIG. 10. **Alignment of the functionally assigned PhaGs.** *PhaG-Pp*, *Pseudomonas putida* transacylase; *PhaG-Po*, *Pseudomonas oleovorans* transacylase; *PhaG-Ps*, *Pseudomonas* sp. 61-3 transacylase; *PhaG-Pa*, *Pseudomonas aeruginosa* transacylase. Matching amino acid residues are indicated by a *colon* or *dot*, and identical residues are marked with an *asterisk*. The putative lipase-box is labeled with *gray* background.

His-192, Asp-223, His-251), which might be involved in enzyme activity. Except Asp-182, all of these residues were conserved among the transacylases and residues Ser-102, Asp-223, and His-251 were also conserved in the α/β-hydrolase fold region (RPS-Blast in the conserved domain data base) by forming the catalytic triad. Residues His-177 and Asp-182 were depicted to investigate the role of the HX_4D motif. The following mutations of PhaG were performed considering conservative and non-conservative replacements and using site-specific mutagenesis: D60(E/A), S102(T/A), H177(R/A), D182(E/A), H192(R/A), D223(E/A), H251(R/A) (Figs. 9–11). All mutants were analyzed with respect to *in vivo* and *in vitro* enzyme activity as described under "Experimental Procedures." For *in vitro* activity analysis of the modified transacylases, the enzymes were purified by refolding from inclusion bodies, which would also indicate folding deficiencies caused by the respective mutations. However, only the site-specific mutants D182E and D182A, respectively, were permissive and showed *in vivo* and *in vitro* transacylase activity (Table IV). *In vivo* activity was achieved by expression of the respective mutated transacylase gene via plasmids (Table I) derived from vector pBBR1MCS-2 in the transacylase-negative mutant *P. putida* $PHAG_N$-21 and by quantitative analysis of the accumulated PHA (Table IV). Furthermore, the composition of the accumulated PHA mediated by these modified transacylases (D182E or D182A), respectively, was significantly shifted toward a higher molar fraction of (*R*)-3-hydroxydodecanoate (Table IV). Interestingly, the residue Asp-182, whose replacement was permissive, was the only investigated amino acid residue position, which was located at the protein model surface (Fig. 11).

Kinetic Analysis of Wild Type and Mutant PhaG Enzymes—To quantify the impact of the D182E and D182A mutations on the catalytic activity of the *P. putida* PhaG, the steady-state kinetic parameters of the wild type enzyme and the single mutants were measured as described under "Experimental Procedures." In the presence of holo-ACP as the acceptor thiol, the estimated V_{max} value of the two mutants was about 40% less, respectively, when compared with the wild type enzyme, which was consistent with reduced *in vivo* activity (Table IV).

DISCUSSION

In this study, we performed for the first time the biochemical and enzymological characterization of an (*R*)-3-hydroxyacyl-ACP:CoA transacylase. The transacylase from *P. putida* was obtained at high yield by heterologous overexpression of the transacylase gene *phaG* in *E. coli*. Only, the C-terminal His_6 tag fusion resulted in an active enzyme, whereas the N-terminal His_6 tag fusion did strongly impair enzyme activity (Table II). This was consistent with a rather conserved N terminus and a less conserved C terminus of PhaG, which indicated a functional role of the N terminus of the enzyme (Fig. 10). Active enzyme was quantitatively obtained from inclusion bodies employing the C-terminal His_6 tag fusion of PhaG and Ni^{2+}-

nitrilitriacetic acid-agarose affinity chromatography under denaturing conditions followed by refolding during gel filtration chromatography, which describes a new strategy for efficient refolding (Fig. 3). CD analysis confirmed the proper refolding of His_6-PhaG (Fig. 4).

The deconvolution of the CD data resulted in a prediction of the secondary structure of ~29% α-helix, 22% β-sheet, 18% β-turn, and 31% random coil. This value is consistent with the threading model developed for PhaG in this study, which is based on structural similarities to an epoxide hydrolase belonging to the α/β-hydrolase superfamily. The determination of the molecular weight of the refolded His_6-tagged PhaG indicated that at low PhaG concentrations the monomer is present, whereas at higher PhaG concentrations, as required for dynamic light scattering analysis, evidence for a dimeric organization was found (Figs. 5 and 6). The autocorrelation function shown in Fig. 6 can only be fitted using a bimodal function. The bimodal fitting procedure identifies two species of significantly different hydrodynamic radius. One is obviously water (R_H = 0.11 nm). The second species is found to be the protein with a hydrodynamic radius of 3.39 nm and a molecular mass of 68 kDa, when assuming validity of the Stokes Einstein equation. The mass is slightly higher than that of a dimer of the transacylase (67.8 kDa). Assuming an equilibrium constant of dimerization in the range of $6Ÿ10^4$ liter mol^{-1} to $4Ÿ10^5$ liter mol^{-1} the monomer would not be detectable in our instrument as its concentration is below the minimal concentration of 0.215 mg ml^{-1} required for a reliable signal. The dimer on the other hand would not be detectible in gel filtration chromatography as its concentration would be below 5 μg ml^{-1} at the applied total protein concentration of 50 μg ml^{-1}. This explanation provides a rationale for the different molar masses observed by gel filtration and DLS. Moreover, in the presence of the substrate (*R*)-3-hydroxyacyl-CoA the transacylase appeared in apparent molecular weights of 45.4, 83.7 and 102, which indicated substrate-induced conformational changes and oligomerization of the transacylase (Fig. 5). A new enzyme assay was established for the transacylase, which implemented the thiol reagent DTNB for monitoring of released CoA and which allowed the first kinetic analysis of PhaG (Fig. 7). The enzymological characterization of the transacylase showed that the 3-hydroxyacyl transfer to holo-ACP, catalyzed by His_6-PhaG, gave $K_{0.5}$ values of 28 μM (ACP) and 65 μM (3-hydroxyacyl-CoA) considering V_{max} values of 11.7 milliunits/mg and 12.4 milliunits/mg, respectively. A Hill coefficient of 1.38 (ACP) and 1.32 (3-hydroxyacyl-CoA) indicated a positive substrate cooperativity (Fig. 8), which is consistent with substrate-induced conformational changes observed by gel filtration chromatography (Fig. 5).

All known acyl transferases involved in fatty acid and polyketide biosynthesis are homologous. Mutational, biochemical, and structural studies have established the centrality of two universally conserved residues: a serine residue (corresponding to Ser-102 in the *P. putida* transacylase) and a histidine residue (corresponding to His-255 in the *P. putida* transacylase). The catalytic cycle of acyl transferases, such as *e.g.* the malonyl-CoA:ACP transacylase involves a ping-pong mechanism in which an acyl group is first transferred from a CoA thioester onto the serine residue, followed by transesterification of this acyl group onto the pantetheine arm of an ACP (24). Consistent with this prediction, x-ray crystallographic analysis of the malonyl-CoA:ACP transacylase from the *E. coli* fatty acid synthase revealed that the conserved serine and histidine residues lie in the active site of the enzyme and are hydrogen bonded in a fashion similar to various serine hydrolases (25). Finally, mutagenesis of acyl transferase domains in modular polyketide synthases (26) and fatty acid synthase systems (27) has confirmed the requirement of this serine for acyl transferase activity. The PhaG transacylases, however, appear to catalyze a similar reaction by transferring a 3-hydroxyacyl moiety from the holo-ACP thioester to CoA. Interestingly, these transacylases exhibit only weak homology of about 10% identity to the acyl transferases. In this study, we were guided by the strong similarity between primary amino acid sequences of various members of this family of proteins (Fig. 10) as well as to α/β-hydrolases (Figs. 9 and 10). The multiple alignments indicated that eighteen amino acid residues are conserved among the transacylases and α/β-hydrolases. More-

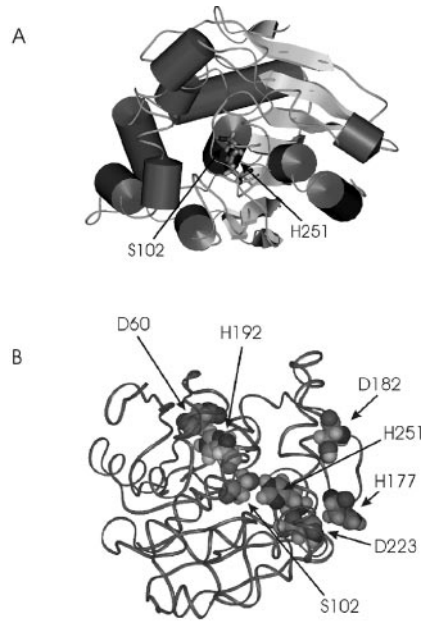

FIG. 11. **Structural model of transacylase PhaG from *P. putida*.** *A*, the threading model of PhaG from *Pseudomonas putida*. The threading model was developed based on the alignment shown in Fig. 9. The software packages Homology and Discover (Molecular Simulations) were applied to generate the model. *Cylinders* represent α-helical structures. *Large arrows* in *dark gray* represent β-strands. The putative catalytic residues were given as *stick* side chains or *CPK* models and indicated by *arrows*. *B*, localization of the single amino acid residue replacements in the PhaG model. Amino acid residue replacements were achieved by site-specific mutagenesis (see Table IV). Only the backbone of the PhaG model is shown. The replacing side chains are given as *CPK format*. *C*, the spatial arrangement of the functionally analyzed amino acid residues was given by representing the respective side chains in *stick format*.

TABLE III
Inhibition of the His_6-PhaG activity by PMSF and DEPC

Inhibitor Concentration	Preincubation with (*R*)-3-hydroxydecanoyl-CoA	Percentage inhibition
mM	μM	
PMSF		
0	–[a]	0
0.5	–	43
1	–	70
2	–	72
2	100	65
2	500	55
DEPC		
0	–	0
0.5	–	34
1	–	41
2	–	43
2	100	25
2	500	10

[a] No addition.

TABLE IV

Relative in vivo activities and in vivo substrate specificities of the various site-specific mutants of the transacylase

Cultivations were performed under PHA-accumulating conditions on mineral salt medium containing 1.5% (w/v) sodium gluconate and 0.05% (w/v) ammonium chloride. Cells were grown for 48 h at 30 °C. PHA content and composition of comonomers were analyzed by GC/MS. 3HHx, 3-hydroxyhexanoate; 3HO, 3-hydroxyoctanoate; 3HD, 3-hydroxydecanoate; 3HDD, 3-hydroxydodecanoate. A relative *in vivo* activity of <5% will be considered as no transacylase activity.

Plasmid	*In vivo* transacylase activity	*In vivo* substrate specificity [PHA composition]			
		3HHx	3HO	3HD	3HDD
	%		mol%		
pMCS2phaGPp	100.0	2.5	24.1	68.7	4.7
pBBR1MCS-2	2.0	nd[a]	8.2	47.2	44.6
pNH1-D60A	2.6	nd	11.0	52.4	36.6
pNH2-D60E	3.5	nd	11.3	58.8	29.9
pNH3-S102A	4.3	nd	11.7	58.0	30.3
pNH4-S102T	4.3	nd	8.0	58.3	33.7
pNH5-H177A	2.6	nd	11.2	53.3	35.5
pNH6-H177R	4.8	nd	8.4	63.3	28.3
pNH7-D182A	30.2	2.0	9.6	73.7	14.7
pNH8-D182E	30.0	4.6	16.5	60.5	18.4
pNH9-H192A	3.1	nd	10.9	53.1	36.0
pNH10-H192R	4.2	nd	9.4	58.8	31.8
pNH11-D223A	2.5	nd	9.1	49.0	41.9
pNH12-D223E	2.5	nd	9.9	48.1	42.0
pNH13-H251A	1.9	nd	8.1	44.1	47.8
pNH14-H251R	1.9	nd	11.8	47.3	40.9

[a] nd, Not detectable.

over all transacylases share a putative lipase box (S*X*[S]*X*G) in which the first G residue of the lipase is replaced by a serine in the transacylase.

In this study, we developed a threading model of the (*R*)-3-hydroxyacyl-ACP:CoA transacylase from *P. putida* based on the homology to the mouse epoxide hydrolase (1cqz), whose structure has been determined by x-ray analysis (28). Many of the features of the α/β-hydrolase fold are maintained in the protein model. The central β-sheet in the core of the molecule conforms to the α/β-hydrolase fold (Fig. 11). Moreover, deconvolution of CD spectra predicted a secondary structure composition of PhaG also found in enzymes belonging to the superfamily of α/β-hydrolases. Inspection of the proposed PhaG model showed that the residues Ser-102, His-251, and Asp-223 are located adjacent to the core structure of PhaG protein model and forming a catalytic triad with the putative catalytic Ser-102 located at the nucleophile elbow (Fig. 11). This putative active-site Ser-102 lies at the C-terminal end of a β-strand, corresponding to strand β5 of the lipases, in the strand-turn-helix motif. These three residues were replaced by site-directed mutagenesis, which abolished transacylase activity, indicating an essential role of these residues in enzyme catalysis. However, site-directed mutagenesis of the amino acid residues Asp-60 and His-192, respectively, which are conserved among the transacylases and which might also play a role in constitution of the catalytic triad, resulted also in inactivation of the enzyme. These residues, which are required for enzyme catalysis, are also located in the core structure of the PhaG model (Fig. 11). Inhibition studies with serine- and histidine-specific inhibitors indicated that Ser-102 and one of the essential histidine residues is involved in enzymatic activity (Table III). The conserved His-177 and the non-conserved Asp-182, which constitute the putative HX_4D motif found in glycosyl transferases, were replaced by site-specific mutagenesis in order to evaluate the functional role of this motif in PhaG. The non-conserved Asp-182 was not required for enzyme activity, but is involved in substrate binding as indicated by a shift in substrate specificity toward longer medium chain length (*R*)-3-hydroxyacyl-CoAs by the PhaG mutants D182A and D182E, respectively (Table IV). Both mutants still exhibited about 30% wild type activity suggesting that the HX_4D motif found in most transacylases does not exert a specific function. The amino acid residue His-177 was required for enzyme activity, which was indicated by the loss of enzyme activity in the PhaG mutants H177A and H177K, respectively. Overall, this study suggests that this new family of transacylases, which catalyzes *in vivo* the transfer of an acyl moiety from holo-ACP to CoA, exerts a reaction mechanism similar to serine hydrolases and acyl transferases.

REFERENCES

1. Rehm, B. H. A., Krüger, N., and Steinbüchel, A. (1998) *J. Biol. Chem.* **273,** 24044–24051
2. Hoffmann, N., Steinbüchel, A., and Rehm, B. H. A. (2000) *FEMS Microbiol. Lett.* **184,** 253–259
3. Hoffmann, N., Steinbüchel, A., and Rehm, B. H. A. (2000) *Appl. Microbiol. Biotechnol.* **54,** 665–670
4. Matsumoto, K., Matsusaki, H., Taguchi, S., Seki, M., and Doi, Y. (2001) *Biomacromolecules* **2,** 142–147
5. Fiedler, S., Steinbüchel, A., and Rehm, B. H. A. (2000) *Appl. Environ. Microbiol.* **66,** 2117–2124
6. Rehm, B. H. A., Mitsky, T. A., and Steinbüchel, A. (2001) *Appl. Environ. Microbiol.* **67,** 3102–3109
7. Bullock, W. O., Fernandez, J. M., and Stuart, J. M. (1987) *BioTechniques* **5,** 376–379
8. Kovach, M. E., Elzer, P. H., Hill, D. S., Robertson, G. T., Farris, M. A., Roop, R. M., II, and Peterson, K. M. (1995) *Gene* (*Amst.*) **166,** 175–176
9. Tabor, S., and Richardson, C. C. (1985) *Proc. Natl. Acad. Sci. U. S. A.* **82,** 1074–1078
10. Sambrook, J., Fritsch, E. F., and Maniatis, T. (1989) *Molecular Cloning: A Laboratory Manual*, 2nd Ed. Cold Spring Harbor, NY
11. Rehm, B. H. A., and Hancock R. E. W. (1996) *J. Bacteriol.* **178,** 3346–3349
12. Bohm, G., Muhr, R., and Jaenicke, R. (1992) *Prot. Eng.* **5,** 191–195
13. Towbin, H., Staehelin, T., and Gordon, J (1979) *Proc. Natl. Acad. Sci. U. S. A.* **76,** 4350–4354
14. Miles, E. W. (1977) *Methods Enzymol.* **47,** 431–442
15. Brandl, H., Gross, R. A., Lenz, R. W., and Fuller, R. C. (1988) *Appl. Environ. Microbiol.* **54,** 1977–1982
16. Timm, A., and Steinbüchel, A. (1990) *Appl. Environ. Microbiol.* **56,** 3360–3367
17. Lipmann, F., and Tuttle, D. (1950) *Biochim. Biophys. Acta.* **4,** 301–309
18. Ellman, G. L. (1959) *Arch. Biochem. Biophys.* **82,** 70–77
19. Laskowski, R. A., MacArthur, M. W., and Thornton, J. M. (1993) *J. Appl. Cryst.* **26,** 283–291
20. Lüthy, R., Bowie, J. U., and Eisenberg, D. (1992) *Nature* **356,** 83–85
21. Karplus, K., Barrett, C., and Hughey, R. (1998) *Bioinformatics* **14,** 846–856
22. Kelley, L. A., MacCallum, R., M., and Sternberg, J. E. (1999) in *The Association for Computing Machinery* (Istrail, S., Pevzner, P., and Waterman, M., eds), New York
23. Fischer, D., and Eisenberg, D. (1996) *Protein Sci.* **5,** 947–955
24. Joshi, V. C., and Wakil, S. J. (1971) *Arch. Biochem. Biophys.* **143,** 493–505
25. Serre, L., Verbree, E. C., Dauter, Z., Stuitje, A. R., and Derewanda, Z. S. (1995) *J. Biol. Chem.* **270,** 12961–12964
26. Gokhale, R. S., Lau, J., Cane, D. E., and Khosla, C. (1998) *Biochemistry* **37,** 2524–2528
27. Joshi, A. K., Witkowski, A., and Smith, S. (1998) *Biochemistry* **37,** 2515–2523
28. Argiriadi, M. A., Morisseau, C., Hammock, B. D., and Christianson, D. W. (1999) *Proc. Natl. Acad. Sci. U. S. A.* **96,** 10637–10642